RSC Advances

RSC Publishing

PAPER

View Article Online
View Journal | View Issue

Cite this: *RSC Advances*, 2013, **3**, 12641

Difference in the cooperative interaction between carbon nanotubes and Ru particles loaded on their internal/external surface

Li Wang, Jiuling Chen, Lei Ge, Victor Rudolph and Zhonghua Zhu*

Received 13th March 2013,
Accepted 24th May 2013

DOI: 10.1039/c3ra41208c

www.rsc.org/advances

This paper examines differences in the cooperative interaction between carbon nanotubes (CNTs) and Ru particles loaded on their internal/external surface. The techniques used were transmission electron microscopy, X-ray photoelectron spectroscopy, CO chemisorption, X-ray diffraction, N_2 physisorption, hydrogen temperature-programmed reduction and two probe catalysis reactions, namely ammonia decomposition and preferential oxidation of CO in H_2-rich atmosphere (PROX). The results show that the loading of highly dispersed Ru particles on CNTs does not change the structure of the CNTs. The cooperative interaction between Ru particles and associated CNT surfaces is dependent on the position of Ru particles and the surface functional groups of CNTs. Due to the electron-deficient structure of Ru particles confined inside CNT channels, they have an inferior ammonia decomposition activity to those deposited on the CNT external surface. For PROX, the catalytic performance of Ru particles confined inside CNT channels is superior compared to that over Ru particles deposited outside CNTs, which we attribute to the selective reactant enrichment of CO over H_2 inside the CNTs.

1 Introduction

Since their discovery by Iijima in 1991,[1] carbon nanotubes (CNTs) have been amongst the most actively investigated materials in physics and chemistry. CNTs have unique properties, such as large surface area, high thermal stability, excellent electrical conductivity and well-defined structure with inner hollow cavities and high aspect ratio, which make them extremely attractive in many potential fields, such as energy storage, electronics and catalysis.[2–4] After their decoration with suitable transition metals (Pt, Pd, Ru, Ag, Ni, Au, *et al.*), CNTs have been found to be active as heterogeneous catalysts in hydrocarbon processing[5–7] and electrode reactions of fuel cells,[8] to show a high hydrogen storage capacity,[9] and to be very sensitive in optical and electronic applications as chemical sensors.[4] An understanding of the cooperative interaction between CNTs and the loaded metal particles may provide means to enhance their performance in various applications.

The well-defined tubular structure of CNTs provides an opportunity for confining metal particles inside the nanochannels. The curvature of planar graphene layers into cylinders induces electron transfer from the concave inner surface to the convex outer surface, leading to differences in the charge structure and electronic properties of decorating metal particles, depending on whether they are located on the external CNT surface or inside CNT channels.[10,11] Also, the nanochannels have been found to be able to enrich some gas molecules, creating a locally higher pressure of reactants inside the channels of CNTs.[12,13] Both electron density difference and gas molecule enrichment can change the performance of metal particles in their applications such as catalysts and chemical sensors. However, up to now, even though some studies have been carried out to compare the performance of metal particles loaded on internal/external surface of CNTs,[14–18] the influence of metal particle location on the structure of the materials and their performance has not been investigated in detail, particularly to explore correlations between the loading positions of metal particles on CNTs and the metal particle performance. In this investigation, Ru was employed as the transition metal catalyst. It was loaded onto the CNTs by the impregnation method. Our previous study showed that on the purified CNTs, Ru particles were located on the external surface, but that after pretreating the CNTs by either catalytic oxidation or acid oxidation, the majority of Ru nanoparticles could be filled inside the nanotube channels.[19] By using purified CNTs, catalytic oxidised CNTs and acid oxidised CNTs to support Ru particles, we have studied the effect of Ru loading position over the internal/external surface of CNTs on the structure of Ru/CNTs and the cooperative interaction between CNTs and Ru particles. This has been characterised using TEM and H_2-TPR, as well as probe catalytic reactions. Two probe catalytic reactions, namely ammonia decomposition and preferential oxidation of CO in H_2-rich atmosphere (PROX), were

School of Chemical Engineering, The University of Queensland, Brisbane, QLD 4072, Australia. E-mail: z.zhu@uq.edu.au; Fax: +61733654199; Tel: +61733653528

employed. Ammonia decomposition was chosen since it is an electron-sensitive process, while PROX was selected because CO and H_2 might be enriched in the nanochannels of CNTs, which could change its activity and selectivity.

2 Experimental

2.1 Sample preparation

CNTs produced by methane decomposition over Fe catalysts in a fluidized-bed reactor were supplied by Tsinghua University, China (purity of as-received MWCNTs above 95 wt.%). The external diameter of the CNTs is 10–30 nm, with most of the nanotubes around 20 nm wide. The inner diameters of these CNTs are typically one third of the corresponding external diameters. The as-received CNTs were purified with 5 M HNO_3 at 110 °C for 5 h to remove amorphous carbon and residual Fe catalyst. The purified CNTs were denoted as P-CNTs. To introduce some surface oxygen functional groups and open the tube caps for Ru filling, two methods – acid oxidation with a mixture of concentrated H_2SO_4 (98 vol.%)–HNO_3 (70 vol.%) at a volume ratio of 3 : 1 and catalytic oxidation by Ag catalysts at 350 °C for 30 min – were employed to treat P-CNTs, following procedures reported before.[19] The corresponding CNT samples are identified as AOX and COX, respectively.

The loading of Ru on CNTs was carried out by the wet impregnation method. CNT samples (50 mg) were dispersed in a 7.5 ml solution of $RuCl_3$ in acetone (to achieve Ru loading of nominally 2 wt.%) by sonication for 100 min. After ultrasonic treatment the mixture was stirred at room temperature until the acetone evaporated. The $RuCl_3$/CNTs samples were heated at 1 °C min^{-1} to 110 °C in air, held at 110 °C for 11 h, and then reduced at 450 °C for 5 h in a flow of H_2/Ar. The catalysts so obtained are identified as Ru/P-CNTs, Ru/AOX and Ru/COX.

2.2 Characterization

The actual Ru loadings on CNTs were determined by a Varian Vista Pro inductively coupled plasma optical emission spectrometer (ICP-OES) using a Sturman-Masters spray chamber and a V-groove nebulizer.

A JEOL JEM-2100 transmission electron microscopy (TEM) with an accelerating voltage of 200 kV was used to observe the loading position of Ru particles and their particle size. The samples were dispersed by sonication in a mixture of ethanol and isopropanol, then deposited on a holey carbon TEM grid and dried.

A PHI-560 ESCA (Perkin Elmer) X-ray photoelectron spectroscope (XPS) was used to measure the filling efficiency (percentage of Ru particles located inside the CNT nanochannels) and the elemental composition on the surface using a non-monochromatic Mg-Kα excitation source at 15 kV.

A Belcat instrument with thermal conductivity detector (TCD) was applied to measure the Ru dispersion by CO pulse chemisorption in a U-shaped quartz reactor. Fifty milligrams of sample was used for each test. Before the measurement, the sample was reduced in H_2 at 200 °C for 30 min and then purged with He for 10 min. After the purge, the sample was cooled to 50 °C. In He at 50 °C, a gas mixture of 5% CO/He was then injected using a six-way valve with a loop of 1.0 ml. The pulse injection was repeated until saturation of CO was observed. The adsorbed moles of CO was measured and used to calculate the dispersion of Ru particles. The stoichiometry factor of CO/Ru is assumed to be 1 in our study.

The influence of Ru loading on CNT structure was studied using a Bruker advanced X-ray diffractometer and a Micromeritics TriStar 3020 nitrogen physisorption instrument. The powder X-ray diffraction was performed using 40 kV, 30 mA with Cu-Kα (λ = 0.15406 nm) radiation and graphite monochromator at a scanning rate of 1° min^{-1} from 10° to 80°. N_2 adsorption isotherms of the samples were obtained at −196 °C, after degassing samples for 24 h at 175 °C. The corresponding specific surface areas (S_g) were calculated by the Brunauer–Emmett–Teller (BET) equation at relative pressure (P/P^o) between 0.05 and 0.35.

The interaction between Ru particles and CNTs was characterised using a temperature programmed reduction with hydrogen (H_2-TPR) process in the Belcat instrument. Prior to each measurement, the sample of 50 mg was heated to 110 °C at a heating rate of 10 °C min^{-1} under an Ar flow of 50 ml min^{-1} (STP), and held at the temperature for 60 min to remove any adsorbed water. Then the temperature was decreased to 50 °C, and the gas flow was switched to 5% H_2/Ar at a flow rate of 30 ml min^{-1} (STP). Finally, TPR profiles were obtained with a temperature ramp of 10 °C min^{-1}. Before entering the TCD, the gas flow from the TPR reactor was passed through a trap filled with zeolite to eliminate water produced during the reduction process.

2.3 Catalysis performance

The activities of three Ru/CNTs samples in two probe reactions, ammonia decomposition and PROX, were tested to investigate the influence of the loading position of Ru particles on the electronic interaction between Ru and CNTs and the catalytic performance. For ammonia decomposition, 0.1 g of catalyst sample was placed in a 8 mm inner diameter vertical quartz tube reactor. The detailed test procedure was reported previously.[20] PROX reactions were performed in a vertical stainless steel tube reactor (7.5 mm inner diameter), with 0.2 g catalyst, a feed gas containing 1 vol.% CO, 1 vol.% O_2, 15 vol.% CO_2, 20% vol.% He, balanced in H_2. The detailed procedure is reported elsewhere.[21] Specifically, CO_2 selectivity is defined as the ratio of O_2 consumption for CO oxidation over the total O_2 consumption.

Both reactions were performed at atmospheric pressure and the temperature was measured using a thermocouple inserted into the catalyst bed. Each reaction temperature was maintained for at least 1 h to obtain the steady state. Blank activity test showed that pure CNT support exhibited no obvious catalytic activity in both ammonia decomposition and PROX reaction over the whole investigated temperature range.

3 Results and discussion

3.1 Position and dispersion of Ru particles

The actual loading contents of Ru, characterised by ICP, are listed in Table 1. As expected, they are quite similar, ranging from 1.5 to 1.8 wt.% in the three catalysts.

Table 1 Ru loading, dispersion and filling efficiency of Ru/CNTs samples

Sample	Ru (wt.%)	Dispersion (%)[a]	Filling efficiency (%)[b]
Ru/P-CNT	1.7	13.6	—
Ru/COX	1.5	13.1	80
Ru/AOX	1.8	13.3	75

[a] derived from CO chemisorption. [b] from previous study.[19]

Fig. 1 presents the TEM images of Ru particles loaded on different CNT samples. In P-CNTs, the particles are located on the external surface of nanotubes, while in the other two samples the particles are mostly confined inside the channels of nanotubes. The TEM examination at lower magnification shows that P-CNTs are several microns in length and with closed caps (images not shown); therefore, Ru nanoparticles cannot fill into the tube channels of P-CNTs. Either acid oxidation or catalytic oxidation of the CNTs can cut the nanotubes and open the tube ends for Ru filling. The detailed Ru filling process, which is influenced by nanotube lengths as well as surface functional groups and defects on CNTs was in the subject of our previous study using XPS and TEM.[19] The quantified filling efficiency is 80% and 75% for Ru/COX and Ru/AOX, respectively (Table 1). In addition, from visual inspection of the TEM images, the Ru particles in all three samples appear homogeneously dispersed, regardless of particle locations. Most of the Ru nanoparticles fall into a size range of 1–3 nm. CO chemisorption tests (Table 1) show Ru dispersion at 13.1–13.6% for all samples, which further confirms that there is no obvious difference in the metal dispersion of CNT-supported Ru catalysts with varied Ru locations. This is in consistent with the results reported by Guo *et al.*[18]

It has been reported that surface functional groups on CNTs are advantageous to anchor the metal particles and improve their dispersion.[22–24] The amount of oxygen-containing functional groups on Ru/CNTs samples was measured by XPS, see Table 2. The oxygen concentration of CNT supports before Ru loading is also listed for comparison. AOX presents the highest oxygen amount, followed by P-CNTs. The refluxing in acid solution generates functional groups on the sidewalls and tube tips of CNTs; since a higher acid concentration was employed during the treatment of AOX than for P-CNTs, the former has more oxygen functional groups than the latter. The catalytic oxidation could produce some carbonyl groups at the catalytic sites. However, the oxidation at 350 °C also induces the decomposition of less thermally-stable oxygen groups, such as carboxyls which serves to offset this.[19] On the other hand, all the Ru/CNTs samples have fewer oxygen functional groups than their corresponding supports owing to their decomposition at the high temperature calcination and reduction processes. The oxygen contents of Ru/P-CNTs and Ru/COX are similar, though a little lower than that of Ru/AOX. It also seems that the presence of more surface oxygen-containing functional groups cannot provide higher dispersion of Ru particles on AOX compared to COX and P-CNTs using the current preparation process.

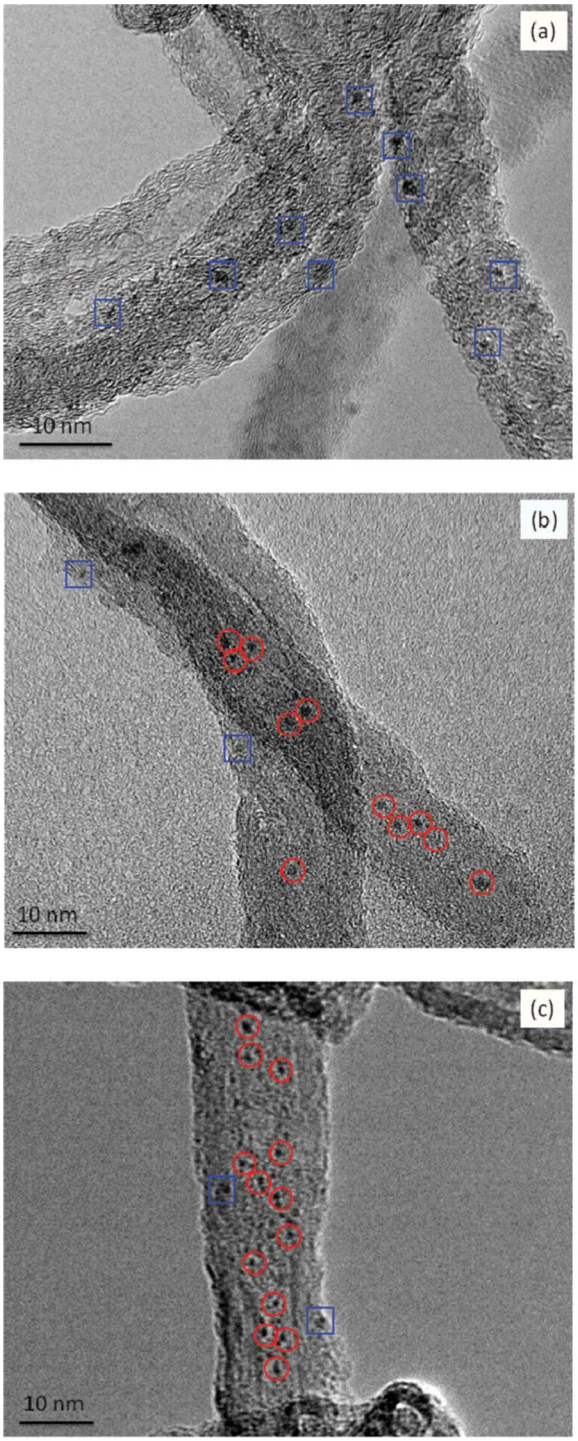

Fig. 1 TEM images of Ru/CNTs samples: (a) Ru/P-CNTs; (b) Ru/COX; (c) Ru/AOX (Blue square: Ru nanoparticles located on the external surface of CNTs; red circle: Ru nanoparticles located inside the nanochannels of CNTs.).

3.2 Structures of CNTs and Ru/CNTs

The influence of Ru loading on the crystalline structure of CNTs is revealed by XRD, shown in Fig. 2. The diffraction patterns of the three CNT samples (Fig. 2(a)) show a strong reflection and a weak reflection at 2θ = 25.9 and 43.2°, which

Table 2 C/O atomic ratio on CNTs and Ru/CNTs samples determined by XPS

Support	C/O atomic ratio	Catalyst	C/O atomic ratio
P-CNTs	94.9/5.1	Ru/P-CNTs	97.7/2.3
COX	95.5/4.5[19]	Ru/COX	97.7/2.3
AOX	88.5/11.5[19]	Ru/AOX	96.2/3.8

can be ascribed to the (002) and (100) planes, respectively, of graphite. COX and AOX exhibit similar XRD patterns to P-CNTs, indicating that the oxidative treatment does not change the crystalline structure of CNTs. On the other hand, no diffraction peak corresponding to Ru phase is observed in Ru/CNTs samples (Fig. 2(b)), which implies the high dispersion of Ru nanoparticles on all the three CNT supports, as shown in Fig. 1.

Fig. 3 shows the nitrogen physisorption isotherms of CNT supports and catalysts. All CNT supports exhibit a type IV isotherm based on IUPAC classification,[25] suggesting the existence of mesopores in them. The isotherms of Ru/CNTs look similar to that of the corresponding CNTs, which indicates that the mesoporous structure has been maintained after Ru loading and reduction. The BET surface areas are 140, 186, and 174 $m^2\ g^{-1}$ for P-CNTs, COX and AOX, respectively. After Ru deposition, the specific surface areas are 144, 194 and 247 $m^2\ g^{-1}$ for Ru/P-CNTs, Ru/COX, and Ru/AOX. In principle,

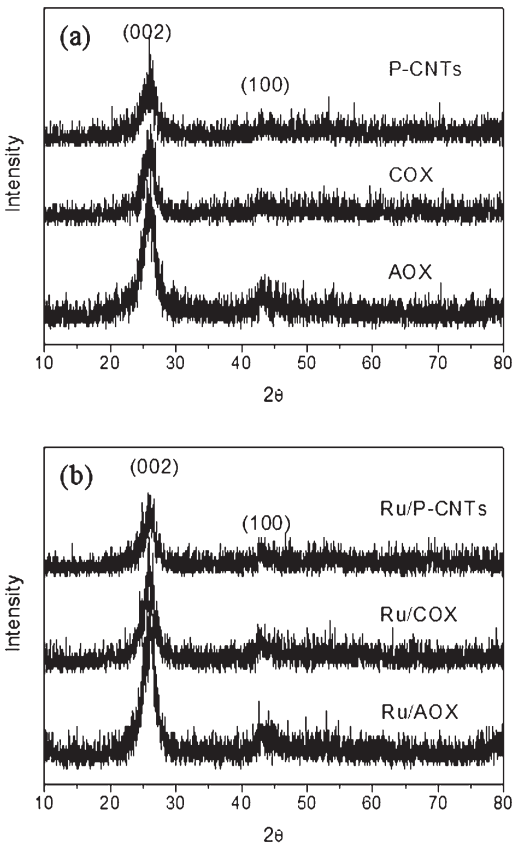

Fig. 2 XRD patterns of (a) CNTs and (b) Ru/CNTs samples.

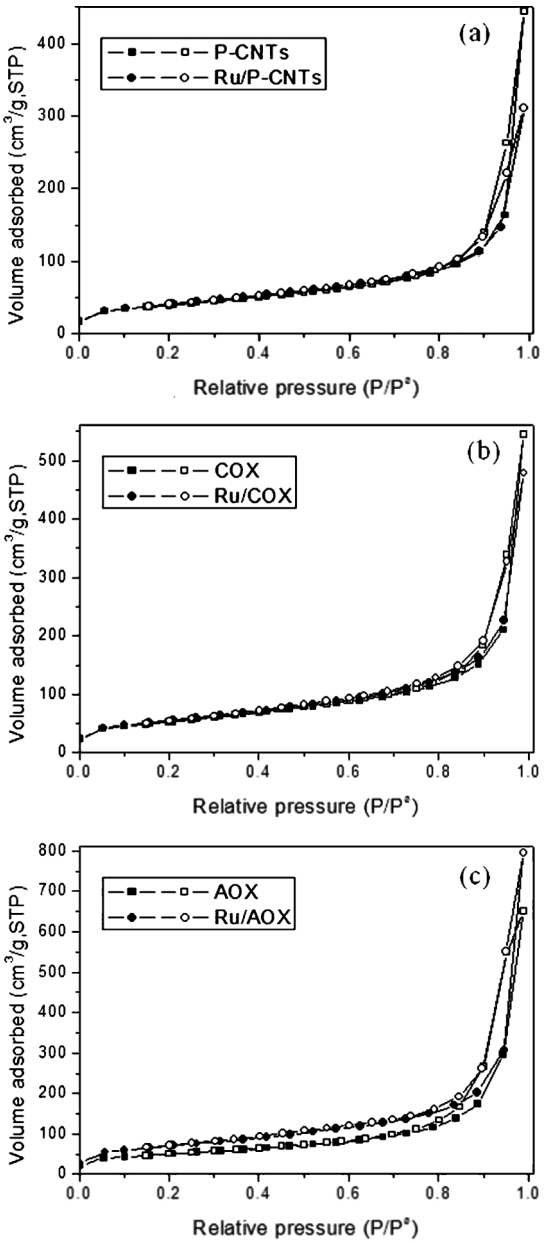

Fig. 3 Nitrogen physisorption isotherms of CNTs and Ru/CNTs samples (Filled symbols: adsorption isotherm; opened symbols: desorption isotherm): (a) P-CNTs, Ru/P-CNTs; (b) COX, Ru/COX; (c) AOX, Ru/AOX.

the highly-dispersed Ru particles at a low loading content cannot change the specific area of supports much. The reason of the obvious increase in the surface area of Ru/AOX by comparison with AOX is still unclear.

3.3 Metal-support interaction

To investigate the interaction between Ru particles and CNTs, H_2-TPR was carried out to probe the reducibility of supported Ru catalysts, as presented in Fig. 4. One can see that there is a sharp H_2 consumption peak followed by a flat shoulder peak in all three samples. The intensive peak at 293 °C for Ru/P-CNTs and Ru/COX, and at 339 °C for Ru/AOX, can be

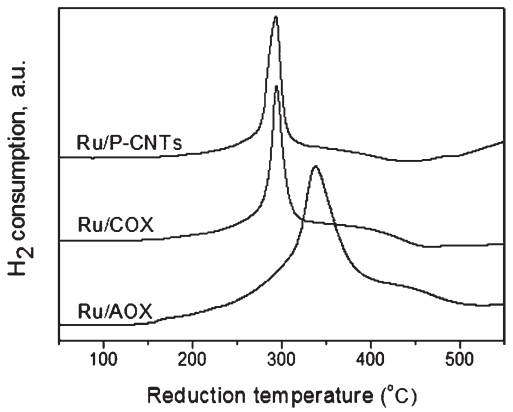

Fig. 4 The TPR patterns of Ru/CNTs samples.

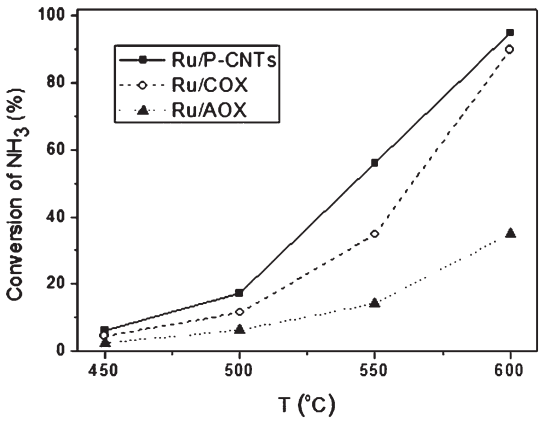

Fig. 5 Catalytic activity of Ru/CNTs samples in ammonia composition. Reaction conditions: F_{NH_3} = 42 ml min^{-1}, catalyst amount: 0.1 g.

attributed to the reduction of Ru^{3+} species to metallic Ru. The shoulder peaks in the temperature ranges of 310–430 °C, 315–455 °C and 415–510 °C in Ru/P-CNTs, Ru/COX and Ru/AOX respectively, may be ascribed to the reduction of the remaining thermally stable oxygen-containing functional groups, like quinones and ethers.[26,27]

It has been reported that the metal particles location can impact their reducibility. The metal oxides confined inside CNT channels exhibited lower reduction temperatures compared to those deposited on the outer surface of CNTs due to the electron deficiency of the CNT interior surface.[14,28] The strengthened interaction between the electron-deficient inner surface of CNTs and anionic oxygen of metal oxides led to weakened bonding strength of metal oxide, and therefore, the confined metal oxides inside CNT channels presented a higher reducibility than those located on the exterior surface of CNTs.[12] However, in our study, Ru/COX with Ru particles mostly confined inside CNTs shows a similar reduction temperature to Ru/P-CNTs with Ru species deposited on the external surface. This may be because the diffusion process of hydrogen molecules (the reductant) into the channels shifts the reduction peak to higher temperature ranges. Other researchers also observed similar reduction temperatures regardless of the location of Ru species if the metallic Ru was directly reduced from Ru^{3+} species.[15] By comparison with Ru/P-CNTs, Ru/AOX exhibits a wider reduction peak at higher temperature. Besides the hydrogen diffusion effect, the interaction between Ru particles and CNT surface could be stronger in Ru/AOX than in the other two samples due to the presence of more acidic surface functional groups, which may hinder the reduction process of Ru, on AOX.[22,29,30]

3.4 Catalytic performance

Fig. 5 shows ammonia conversion rate at different reaction temperatures over various Ru/CNTs samples. The conversion rate of ammonia exhibits an upward trend with reaction temperature increment. Also, the three catalysts present an activity order of Ru/P-CNTs > Ru/COX > Ru/AOX. Ru/P-CNTs exhibits the highest activity. Taking the reaction temperature of 600 °C as an example, 95% of ammonia can be decomposed over Ru/P-CNTs, which is 5% greater than that over Ru/COX, and almost three times that over Ru/AOX.

The PROX performances of three Ru/CNTs samples are shown in Fig. 6. Over all Ru/CNTs samples, the CO conversion goes up steeply with temperature, reaching full conversion at a

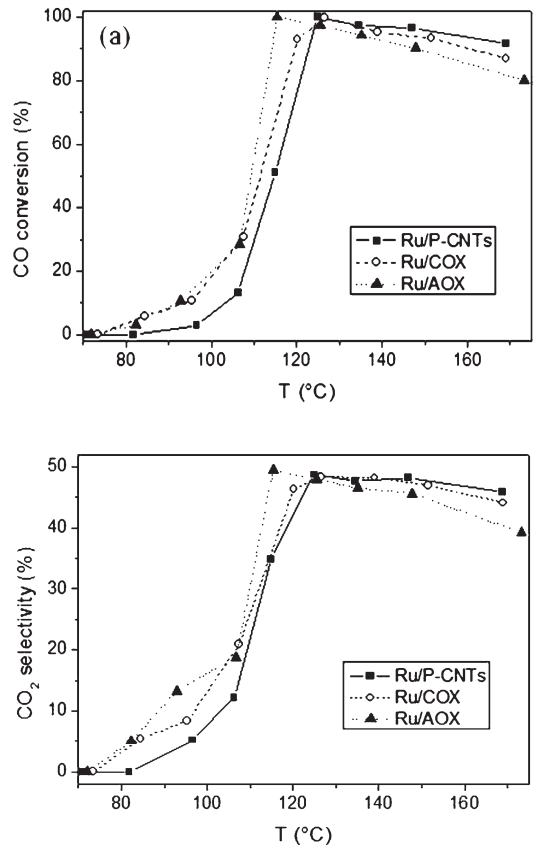

Fig. 6 Catalytic performances of Ru/CNTs samples in PROX: (a) CO conversion, (b) CO_2 selectivity. Reaction conditions: F_{feed}: 63 ml min^{-1}, catalyst amount: 0.2 g, feed gas composition: 1 vol.% CO, 1 vol.% O_2, 15 vol.% CO_2, 20 vol.% He, balanced in H_2.

certain temperature, and then decreases with further temperature increase. Ru/AOX and Ru/COX present similar CO conversion rates at reaction temperatures between 70 and 110 °C, but are significantly higher than that of Ru/P-CNTs. A complete CO conversion is obtained at 115 °C over Ru/AOX, and at around 125 °C for Ru/COX and Ru/P-CNTs. The CO conversion rate goes down with higher temperatures still due to the enhancement of H_2 oxidation with temperature, which was also observed by other researchers.[31–34] Ru/P-CNTs exhibits a higher CO conversion rate than that over Ru/COX and Ru/AOX at reaction temperature above 125 °C. CO_2 selectivity follows a similar trend as that of CO conversion. Ru/AOX and Ru/COX show a higher CO_2 selectivity than that of Ru/P-CNTs at reaction temperature below 120 °C; however, this is reversed at temperatures above 140 °C.

The catalytic performances over various Ru/CNTs show different trends in ammonia decomposition and PROX reaction. Ru/P-CNTs presents the highest ammonia conversion rate in ammonia decomposition, yet the lowest activity and selectivity at reaction temperature below 120 °C in PROX. Ru/AOX, on the other hand, exhibits the lowest reactivity in ammonia decomposition, but the highest CO conversion rate at low reaction temperature in PROX. A moderate catalytic performance is observed over Ru/COX in both reactions.

The loading contents of Ru are quite similar in the three catalysts (Table 1), as are the Ru dispersions as revealed by both TEM and CO chemisorptions. Therefore, the different catalytic activities cannot be attributed to Ru loading content and dispersion. The difference in surface areas may influence the reaction rate, however, opposite reactivity trend over three catalysts is observed in two reactions. Therefore, surface area is not the determining factor of catalytic performance.

Ammonia decomposition is an electron-sensitive reaction and the electron transfer from support to metal catalysts can promote the rate of the rate-determining step namely associative desorption of nitrogen, and thereby increase the whole reaction rate.[35–38] The higher electron density of Ru particles is a favourable state for ammonia decomposition. The remaining oxygen functional groups on the CNTs, which are more electronegative than Ru, can withdraw electrons from Ru, reducing its electron density and so decrease its activity in ammonia decomposition. Although Ru/P-CNTs and Ru/COX possess a similar content of surface oxygen atoms, the activity of the former is higher than that of the latter. The reactivity difference here should result from the influence of confinement effect inside CNTs or different Ru locations affecting the electron density of Ru particles. The curvature of planar graphene layers into cylinders in CNTs induces electron transfer from the concave inner surface to the convex outer surface of CNTs, leading to higher electron density on the CNT external surface than inside CNT channels.[10,11] Therefore, it could be postulated that the Ru nanoparticles confined inside CNTs of Ru/COX would possess lower electron density owing to their location on the relatively electron-deficient inner tube surface, compared to those Ru nanoparticles located on the electron-enriched external CNT surface of Ru/P-CNTs. The electronic structure difference between Ru nanoparticles on the internal surface and those on the external surface of CNTs enables the higher ammonia conversion rate of Ru/P-CNTs compared to Ru/COX. The lower ammonia synthesis activity over Ru-in-CNT than that over Ru-out-CNTs has been reported, and is confirmed by our results.[18] Since Ru/COX and Ru/AOX have similar filling efficiency of Ru particles inside CNT channels, the lower activity of Ru/AOX can be attributed to the higher amount of remaining oxygen atoms on the surface of Ru/AOX.

The PROX results in Fig. 6 show similar CO conversions over Ru/AOX and Ru/COX, which are both higher than that for Ru/P-CNTs at reaction temperature below 120 °C. Ru/P-CNTs has Ru nanoparticles located on the external surface of CNTs, while Ru/COX and Ru/AOX possess most of Ru nanoparticles confined inside the nanochannels. The different metal particle locations result in the variance in the catalytic performance of PROX over the three catalysts. A theoretical study on the interactions of H_2 and CO molecules with CNT surfaces reported that both gases could be enriched inside CNT channels with respect to the outside due to the higher binding energy of CO and H_2 molecules inside CNTs.[39] Interestingly, it was further found that CO was preferentially enriched inside CNTs compared to H_2, resulting a notably higher CO/H_2 ratio inside CNTs compared with outside CNTs. Therefore, the locally higher CO/H_2 and O_2/H_2 ratios inside the nanotube channels of Ru/AOX and Ru/COX relative to those outside nanotubes of Ru/P-CNTs could increase the probability of CO reacting with O_2 and improve the CO_2 selectivity. Similar improvement of PROX reactivity by confining metal nanoparticles inside CNTs has also been reported elsewhere.[15] Also, it is noteworthy that the superior PROX performance of Ru/AOX and Ru/COX over Ru/P-CNTs is only observed at reaction temperature below 120 °C, which might be explained by the weakened selective reactant enrichment with temperature increment.[39]

4 Conclusions

Ru particles were loaded on three CNT supports, P-CNTs, COX and AOX. Most of Ru particles are located on the external surface for P-CNTs, but are confined inside the CNT channels for COX and AOX. The presence of highly dispersed Ru particles does not change the structure of the corresponding CNTs. The remaining oxygen-containing functional groups cannot influence the Ru dispersion among different samples; however, they can enhance the interaction between Ru and CNT surface. The Ru particles located on the external CNT surface show a higher activity in ammonia decomposition than those on the internal CNT surface, which can be due to the higher electron density of the external surface of CNTs. In PROX reaction, Ru/AOX and Ru/COX show higher activity than Ru/P-CNTs because the internal surface of CNTs may be able to enrich CO and H_2 gas molecules and cause a local higher concentration of these reactants inside the nanochannels compared to the outside of CNTs. These findings contribute to the existing knowledge on the cooperative interaction between CNTs and the decorating metal particles to enhance the performance of CNTs in the application fields of interest.

Acknowledgements

This work received financial supported through an Australian Research Council Discovery Project. Li Wang acknowledges financial support from a CSC scholarship from China.

References

1 S. Iijima, *Nature*, 1991, **354**, 56–58.
2 P. Serp, M. Corrias and P. Kalck, *Appl. Catal., A*, 2003, **253**, 337–358.
3 P. Serp and E. Castillejos, *ChemCatChem*, 2010, **2**, 41–47.
4 J. Wang, *Electroanalysis*, 2005, **17**, 7–14.
5 S. Yin, B. Xu, W. Zhu, C. Ng, X. Zhou and C. Au, *Catal. Today*, 2004, **93**, 27–38.
6 M. Trepanier, A. Tavasoli, A. K. Dalai and N. Abatzoglou, *Appl. Catal., A*, 2009, **353**, 193–202.
7 H. Vu, F. Gonçalves, R. Philippe, E. Lamouroux, M. Corrias, Y. Kihn, D. Plee, P. Kalck and P. Serp, *J. Catal.*, 2006, **240**, 18–22.
8 S. Wang, X. Wang and S. P. Jiang, *Langmuir*, 2008, **24**, 10505–10512.
9 G. G. Wildgoose, C. E. Banks and R. G. Compton, *Small*, 2006, **2**, 182–193.
10 R. C. Haddon, *Science*, 1993, **261**, 1545–1550.
11 D. Ugarte, A. Chatelain and W. A. deHeer, *Science*, 1996, **274**, 1897–1899.
12 X. L. Pan and X. H. Bao, *Chem. Commun.*, 2008, 6271–6281.
13 X. L. Pan, Z. L. Fan, W. Chen, Y. J. Ding, H. Y. Luo and X. H. Bao, *Nat. Mater.*, 2007, **6**, 507–511.
14 W. Chen, Z. L. Fan, X. L. Pan and X. H. Bao, *J. Am. Chem. Soc.*, 2008, **130**, 9414–9419.
15 B. D. Li, C. Wang, G. Q. Yi, H. Q. Lin and Y. Z. Yuan, *Catal. Today*, 2011, **164**, 74–79.
16 H. X. Yang, S. Q. Song, R. C. Rao, X. Z. Wang, Q. Yu and A. M. Zhang, *J. Mol. Catal. A: Chem.*, 2010, **323**, 33–39.
17 W. Chen, X. L. Pan and X. H. Bao, *J. Am. Chem. Soc.*, 2007, **129**, 7421–7426.
18 S. J. Guo, X. L. Pan, H. L. Gao, Z. Q. Yang, J. J. Zhao and X. H. Bao, *Chem.-Eur. J.*, 2010, **16**, 5379–5384.
19 L. Wang, L. Ge, T. E. Rufford, J. Chen, W. Zhou, Z. Zhu and V. Rudolph, *Carbon*, 2011, **49**, 2022–2032.
20 L. Wang, J. Chen, L. Ge, Z. Zhu and V. Rudolph, *Energy Fuels*, 2011, **25**, 3408–3416.
21 L. Wang, J. Chen, V. Rudolph and Z. Zhu, *Adv. Powder Technol.*, 2012, **23**, 465–471.
22 F. Rodríguez-reinoso, *Carbon*, 1998, **36**, 159–175.
23 C.-H. Li, K.-F. Yao and J. Liang, *Carbon*, 2003, **41**, 858–860.
24 R. M. Malek Abbaslou, A. Tavasoli and A. K. Dalai, *Appl. Catal., A*, 2009, **355**, 33–41.
25 K. Sing, D. Everett, R. Haul, L. Moscou, R. Pierotti, J. Rouquerol and T. Siemieniewska, *Pure Appl. Chem.*, 1985, **57**, 603–619.
26 S. Kundu, Y. M. Wang, W. Xia and M. Muhler, *J. Phys. Chem. C*, 2008, **112**, 16869–16878.
27 M. Cerro-Alarcón, A. Maroto-Valiente, I. Rodríguez-Ramos and A. Guerrero-Ruiz, *Carbon*, 2005, **43**, 2711–2722.
28 R. M. M. Abbaslou, A. Tavassoli, J. Soltan and A. K. Dalai, *Appl. Catal., A*, 2009, **367**, 47–52.
29 J. Chen, Z. H. Zhu, S. Wang, Q. Ma, V. Rudolph and G. Q. Lu, *Chem. Eng. J.*, 2010, **156**, 404–410.
30 W. Raróg-Pilecka, E. Miśkiewicz, D. Szmigiel and Z. Kowalczyk, *J. Catal.*, 2005, **231**, 11–19.
31 S. Y. Chin, O. S. Alexeev and M. D. Amiridis, *Appl. Catal., A*, 2005, **286**, 157–166.
32 M. Echigo and T. Tabata, *Catal. Lett.*, 2004, **98**, 37–42.
33 S. Y. Chin, O. S. Alexeev and M. D. Amiridis, *J. Catal.*, 2006, **243**, 329–339.
34 G. Avgouropoulos, M. Manzoli, F. Boccuzzi, T. Tabakova, J. Papavasiliou, T. Ioannides and V. Idakiev, *J. Catal.*, 2008, **256**, 237–247.
35 K. i. Aika, H. Hori and A. Ozaki, *J. Catal.*, 1972, **27**, 424–431.
36 K. i. Aika, T. Takano and S. Murata, *J. Catal.*, 1992, **136**, 126–140.
37 S. F. Yin, Q. H. Zhang, B. Q. Xu, W. X. Zhu, C. F. Ng and C. T. Au, *J. Catal.*, 2004, **224**, 384–396.
38 S. J. Wang, S. F. Yin, L. Li, B. Q. Xu, C. F. Ng and C. T. Au, *Appl. Catal., B*, 2004, **52**, 287–299.
39 J. Guan, X. L. Pan, X. Liu and X. H. Bao, *J. Phys. Chem. C*, 2009, **113**, 21687–21692.